International Journal of Nanomedicine

Dovepress
open access to scientific and medical research

Open Access Full Text Article

ORIGINAL RESEARCH

Quantification of Synergistic Effects of Ceragenin CSA-131 Combined with Iron Oxide Magnetic Nanoparticles Against Cancer Cells

This article was published in the following Dove Press journal:
International Journal of Nanomedicine

Ewelina Piktel[1]
Karolina H Markiewicz[2]
Agnieszka Z Wilczewska[2]
Tamara Daniluk[1]
Sylwia Chmielewska[1]
Katarzyna Niemirowicz-Laskowska[1]
Joanna Mystkowska[3]
Paulina Paprocka[4]
Paul B Savage[5]
Robert Bucki[1,4]

[1]Department of Medical Microbiology and Nanobiomedical Engineering, Medical University of Bialystok, Bialystok 15-222, Poland; [2]Faculty of Chemistry, University of Bialystok, Bialystok 15-245, Poland; [3]Department of Materials and Biomedical Engineering, Białystok University of Technology, Białystok 15-351, Poland; [4]Department of Microbiology and Immunology, The Faculty of Medicine and Health Sciences, Jan Kochanowski University in Kielce, Kielce 25-317, Poland; [5]Department of Chemistry and Biochemistry, Brigham Young University, Provo, UT 84604, USA

Correspondence: Robert Bucki
Email buckirobert@gmail.com

Background: Therapeutic efficiency of ceragenins against cancers may be limited by lack of their hemocompatibility when high concentrations of molecules are required to reach a desired result. Synergistic effects observed upon administration of anticancer agents and metal nanoparticles may provide an opportunity to limit toxicity of immobilized ceragenins on the surface of metal nanoparticles and to improve their therapeutic efficiency at the same time. The aim of present work is to investigate the anticancer activities and hemocompatibility of nanoformulations consisting of ceragenin CSA-131 united with aminosilane-modified iron oxide-based magnetic nanoparticles (MNP) and prepared by 1) covalent bonding (MNP@CSA-131) or 2) by combining CSA-131 with MNP in 1:1 ratio (CSA-131 + MNP). Possible synergistic interactions between CSA-131 and magnetic nanoparticles were also quantified.

Methods: MNP@CSA-131 and CSA-131+MNP were tested in vitro against selected lung and colon cancer cells using colorimetric, fluorimetric and flow cytometry methods.

Results: Performed analysis demonstrates that MNP-based nanosystems significantly improve the killing efficiency of tested ceragenin, decreasing the viability of extra 1.37±4.72% to 76.07 ±15.30% cancer cells when compared to free CSA-131. Quantification of synergistic effects indicates the favorable interactions between CSA-131 and magnetic nanoparticles (CI < 1 for all tested doses), revealing at the same time a reduction in effective doses of ceragenin from 1.17 ± 0.61 to 34.57 ± 12.78 times when combined with MNP. We demonstrate that both MNP@CSA-131 and CSA-131+MNP induce significantly apoptosis of cancer cells and prevent the division of colon cancer cells even at relatively low doses of the active compound (10 μg/mL). Importantly, combining CSA-131 with MNP decreases the hemolytic activity of free ceragenin 4.72 to 7.88 times, which indicates a considerable improvement of hemotoxicity profile.

Conclusion: Comparative analyses have revealed that both developed CSA-containing nanoformulations due to the utility of synergistic interactions between MNP and CSA-131, which are effective against lung and colon cancer cells. This indicates the new directions in preparation of MNP-based therapeutics, which are relatively easy to synthetize, cost-effective and safe when intravenously administrated.

Keywords: ceragenins, anticancer activity, colon cancer, lung cancer, synergistic effects, combinatory therapy

Introduction

Differences between surface plasma membranes, such as higher negative membrane potential and increased fluidity, between cancer and healthy cells are associated with interactions that control receptor accessibility and cell adhesion,[1] and these

submit your manuscript | www.dovepress.com
DovePress
http://doi.org/10.2147/IJN.S255170

might be considered as potential targets for anticancer molecules. This possibility is supported by actions of endogenous membrane-active antimicrobial peptides, which have been described as anticancer agents with the capability to selectively kill malignant cells.[2] To date, a number of host defense and synthetic anticancer peptides (ACPs) have been described. These peptides display selective recognition of cancer cells, usually based on electrostatic interactions, resulting in mitochondrial membrane damage, induction of apoptosis and PIP_2-mediated membrane permeabilization and growth inhibition.[1,2] Nevertheless, despite the characterization of numerous peptides with such activity, there is still a need to reduce their side effects, low stability in body fluids and toxicity in relation to healthy cells.[3] Therefore, continued efforts are required to design novel or modified membrane-active compounds with reduced side effects and high therapeutic efficiency. An ever-growing number of studies confirm that ceragenins (CSAs), bile acid-based analogs of antimicrobial peptides, may be considered as anti-neoplastic agents due to their 1) membrane-permeabilizing properties, 2) ability to induce both caspase-dependent and independent apoptosis, 3) introduction of cells into cell cycle arrest and 4) disruption of oxidative balance.[4,5] Importantly, ceragenins CSA-13, CSA-90, CSA-131, and CSA-192 were demonstrated to exert anti-proliferative properties against breast cancer, colon cancer and lung adenocarcinoma, which confirms their non-specific mechanism of killing action.[4,6] Nevertheless, at higher doses, considerable toxicity and hemolytic activity of ceragenins were observed, limiting the therapeutic utility when intravenous administration is required.[7]

Combination chemotherapy of tumors is currently a primary treatment option, allowing for improvement of overall survival rates and simultaneously limiting toxicities and adverse effects, despite ever-growing tumor resistance.[8] Importantly, combined therapies present an opportunity to utilize nanocarrier-based methods.[8] Due to the unique properties of these materials at the nanoscale level, a variety of nanostructures, including metallic nanoparticles have attracted attention in biomedical engineering, particularly as drug delivery systems (DDS), diagnostic tools, antimicrobial agents and anticancer therapeutics.[9–13] A compelling number of reports indicate the possibility of attaching anticancer drugs on the surface of nanoparticles, thereby facilitating drug delivery and increasing drug accumulation in cancer cells, which results in improved therapeutic efficiency of anti-neoplastic agents and potentially overcoming drug resistance.[14] Immobilization techniques used for bioconjugation processes include physical interactions (electrostatic or affinity interactions) and chemical interactions such as covalent bonding.[15] One of the crucial advantages of metallic nanoparticles is their easy, reagent-controllable synthesis and considerable cytotoxicity.[16–19] Among them, iron oxide nanoparticles are characterized by high targetability, relatively easy surface functionalization and strong affinity towards cancer cells and are more stable than organic nanoparticles.[20,21] Importantly, while the safety of bare magnetic nanoparticles might be questionable,[22] their cytotoxicity and genotoxicity might be significantly limited by coating with aminosilane shell.[23] Our previously published reports have shown that covalent attachment of the first-generation ceragenin, CSA-13 to aminosilane-functionalized iron oxide magnetic nanoparticles (MNP) surface significantly improves the killing features of membrane-active compounds with subsequent improvement of their hemocompatibility.[4,6] It was also revealed that simple combining MNP and CSA-13 significantly improves the bactericidal effects against bacteria. Importantly, such nanoformulations are easy to prepare and do not require additional reagents and synthesis steps.[24] Nevertheless, none mathematic quantification of synergistic effects resulting from combining ceragenins with magnetic nanoparticles was performed to date. No study was also performed, in which anticancer effectiveness of ceragenins-containing nanosystems was compared to the efficiency of nanomixtures consisting of CSA-131 co-administrated with MNP.

In agreement with the benefits of combinatory therapy, we aimed to develop an efficient, non-toxic and cost-effective nanoparticles-based formulation, based on iron oxide nanoparticles united with ceragenin CSA-131, a second-generation ceragenin, with some improvements in activity over CSA-13. For this purpose, we compared the efficiency of 1) ceragenin CSA-131 nanoformulation consisting of CSA-131 covalently attached to the surface of iron oxide magnetic nanoparticles (MNP@CSA-131) and 2) combined by simple mixing of two compounds with each other (CSA-131 + MNP) against colon and lung cancer cells. We investigated whether immobilization significantly affects the anticancer activity of membrane-active ceragenin CSA-131 and determined mathematically possible synergistic interactions between CSA-131 and magnetic nanoparticles. Hemocompatibility of such nanoformulations was tested as well. According to our

knowledge, none of those issues were addressed to date, which underlines the novelty of the research presented.

Materials and Methods

Materials

A representative of ceragenins,[25] CSA-131, was synthetized using previously published protocols.[26] Human lung adenocarcinoma A549 (ATCC® CCL-185™) and human Dukes' type C colorectal adenocarcinoma DLD-1 (ATCC® CCL-221™) cells were obtained from the American Type Culture Collection (ATCC, Manassas, VA, USA). High-glucose DMEM (Dulbecco′s Modified Eagle′s Medium) and fetal bovine serum were purchased from ATCC. L-Glutamine, Penicillin-Streptomycin solution (10,000 units penicillin and 10 mg streptomycin/mL), colorimetric and fluorescence probes: MTT; 3-(4,5-dimethylthiazol-2-yl)-2,5-diphenyltetrazolium bromide and resazurin sodium salt, and DAPI dye were from Sigma-Aldrich (Saint Louis, MO, USA). Solution 5 VB-48™ PI – AO was from Chemometec (Allerod, Denmark). Apoptosis estimation was performed using Muse® Annexin V & Dead Cell Kit (Merck, Darmstadt, Germany).

Synthesis of Ceragenin-Decorated Magnetic Nanoformulations

Aminosilane-coated iron oxide particles (MNP) were synthesized according to the published procedure and thoroughly characterized using TEM, XRD, FT-IR, TGA, and magnetization measurements.[27,28] The obtained iron oxide cores (average diameter 10 ± 2 nm) form small clusters surrounded by thin aminosilane shell (~1nm) clearly observed in TEM images.[28] MNP particles (30 mg) were suspended in an aqueous solution of glutaraldehyde (25%, 50 mL) using an ultrasound bath (1 h). After 6 h of mechanical stirring at room temperature, glutaraldehyde-functionalized MNPs were magnetically separated from the solution, washed several times with ethanol, and re-suspended in ethanol containing CSA-131 (10 mL, 3 mg/mL). The mixture was stirred overnight. Then, the particles were magnetically isolated, washed three times with ethanol, and dried to powder at 60°C. The product was analysed by FT IR, TGA and DSC methods. In another approach, CSA-131 was mixed with magnetic nanoparticles in a 1:1 ratio (indicated as CSA-131 + MNP), suspended in phosphate-buffered saline (PBS) and left for 48 h before experiments.

Physicochemical Characterization of Magnetic Nanosystem

The formation of nanosystems, including aminosilane-modified and ceragenin-functionalized magnetic nanoparticles, was evaluated using spectral and thermal techniques. ATR FT-IR spectra were recorded on Nicolet 6700 FT-IR Spectrometer from Thermo Scientific in the range of 4000 to 500 cm^{-1} by co-adding 16 scans with a resolution of 4 cm^{-1}. Thermogravimetric analyses (TGA) were performed on a Mettler Toledo Star TGA/DSC unit. Samples weighing 2–3 mg were placed in aluminum oxide crucibles and heated from 50°C to 900°C at a heating rate of 10 K min^{-1} under an argon flow rate of 20 mL·min^{-1}. Differential scanning calorimetry (DSC) measurements were performed on a Mettler Toledo Star DSC system. A solid-state sample (2–3 mg) was placed in an aluminum crucible, sealed and heated from 25°C to 450°C at a heating rate of 10 K·min^{-1} under an argon flow rate of 200 mL·min^{-1}. An empty aluminum crucible was used as the reference.

Cell Culture

Human lung adenocarcinoma A549 (ATCC® CCL-185™) and human Dukes' type C colorectal adenocarcinoma DLD-1 (ATCC® CCL-221™) cells were cultured in high-glucose DMEM supplemented with 10% fetal bovine serum (FBS), glutamine (2 mM/L), penicillin (50 U/mL) and streptomycin (50 µg/mL) and maintained at 37°C in an atmosphere containing 5% CO_2 with saturated humidity.

Cytotoxicity Assessment

Cell viability after treatment with CSA-131 and ceragenin-containing combinations was estimated using the metabolic activity-assessing tetrazolium test (MTT assay) as described previously.[4] Briefly, $5x10^3$ of both A549 and DLD-1 cells were plated in 96-well plates in 200 µL of media per well and left to cultivate until confluence ~80% was obtained. Next, ceragenin CSA-131, MNP@CSA-131 and CSA-131 + MNP in concentrations ranging from 0 to 50 µg/mL were added in three replicates to each cell population and left for further incubation for 24 h at 37°C. To quantify the viability of cells, the MTT solution at a final concentration of 0.5 mg/mL was added, followed by further incubation for 4 h. The absorbance of MTT-containing samples was measured using Varioscan Lux microplates reader at 540 nm (Thermo Fisher Scientific, Waltham, MA, USA) by the dissolution of formazan by 100 µL of dimethyl sulfoxide (DMSO) and gently shaking.

The absorbance value obtained in cultures of control cells (without tested agents) was taken as 100%. The average of all the experiments has been shown as a cell viability percentage in comparison to the control.

Interaction Assessment

To quantitively evaluate the pharmacological interactions between CSA-131 and magnetic nanoparticles when ceragenin is covalently attracted to MNPs or combined in equal ratio, the combination method of Chou[29] and commercially available CompuSyn software were employed. Antagonism, additive or synergistic interaction between tested compounds was calculated using multiple drug effect equation allowing for the quantitative determination of the combinatory index (CI) and dose-reduction index (DRI). The CI was calculated based on the equation: CI=(D)1/(Dx)1+(D)2/(Dx)2+(D)1 (D)2/(Dx)1(Dx)2, where (Dx)1 and (Dx)2 are the doses of drug 1 and drug 2, alone, inhibiting "x%", whereas (D1) is the dose of drug 1 in combination, and (D2) the dose of drug 2 in a combination that corresponds to the observed "x" inhibition. Accordingly, CI values higher than 1 indicate antagonistic interaction, CI = 1 is an indicator that two drugs have an additive effect and CI < 1 corresponds to synergistic interaction, with the discrimination that values between 1 and 0.76, 0.75–0.3 and <0.3 indicate slight synergistic effects (SlS), synergistic (S) and strong synergistic effects (SS), respectively. CI values were calculated for a broad spectrum of effect levels and on the basis of this analysis, fraction affected (FA) versus CI plots was generated. To evaluate the drug dose in a synergistic combination, dose-reduction index (DRI) was calculated as follows: (DRI) 1=(Dx)1/(D)1 and (DRI)2=(DRI)2/(D)2, where DRI>1 shows that combinations could result in reduced drug doses when compared to doses for each drug alone.

Analysis of Ceragenin-Induced Apoptosis

To qualitatively evaluate the anticancer activities of ceragenin CSA-131 and ceragenin-based formulations and to investigate the mechanisms of detected antineoplastic features, a series of flow cytometry- and fluorimetric-based analyses was employed. In the first, alterations in intracellular glutathione (GSH) levels, being an early hallmark in the progression of cell death in response to different apoptotic stimuli, were investigated. For this purpose, vitality assay (ChemoMetec, Denmark) employing fluorescent dye VitaBright-48™ (VB-48) (reacting with thiols forming a fluorescent product) was performed according to the manufacturer's instructions. By comparing the VB-48™ and propidium iodide (PI) intensities recorded for control and treated cells, the fractions of 1) healthy cells, 2) PI-negative cells with low viability and 3) dead cells can be determined. The proliferation capability of CSA-131-treated cancer cells was measured according to a previously described procedure.[4,30] The externalization of phosphatidylserine (PS) to the cell surface in the response to the treatment with CSA-131 and its MNP-based derivatives, and thus the induction of CSA-mediated apoptosis was assessed using Muse® Annexin V
& Dead Cell Kit (Merck, Germany). Differentiation of early and late apoptotic cells and necrotic cells was performed through the use of a combination of FITC-labeled Annexin V with 7-AAD (7-aminoactinomycin D; indicator of cell membrane structural integrity). Visualization of CSA-131- and MNP@CSA-131-induced DNA fragmentation and investigation of changes in nuclei morphology was performed using fluorescence microscopy (BD Pathway Bioimaging Systems, BD Biosciences, San Jose, CA, USA). For this assay, A549 or DLD-1 cells were seeded in 96-well plates and treated with test agents for 24 h. Cells were then fixed with 4% paraformaldehyde in PBS for 15 min at room temperature. After incubation with 0.1% Triton X-100 in PBS (5 min, room temperature), cells were thoroughly washed and stained with DAPI solution (1 μg/mL) for 5 min at room temperature. All experiments were performed using test agents at a concentration of 10 μg/mL for 24 h.

Hemolysis Assay

Hemocompatibility of test agents was evaluated using a hemolysis assay, which is based on the colorimetric measurement of the amount of hemoglobin released from damaged red blood cells (RBCs). For this purpose, human red blood cells (RBCs), isolated from the blood of healthy volunteers, were suspended in phosphate-buffered saline (PBS) (hematocrit ~5%) with concentrations of test agents ranging from 0 to 100 μg/mL. RBCs were then incubated with analyzed compounds for 1 h at 37°C. Relative hemoglobin concentration in supernatants after centrifugation at 2500 g was monitored by measuring optical absorbance at 540 nm. Complete hemolysis was measured in samples treated with 1% Triton X-100, which disrupts all cell membranes.

Statistical Analysis

Provided data are mean from 3 to 6 independent experiments ± SD. The significance of differences was determined using the two-tailed Student's *t*-test. Statistical

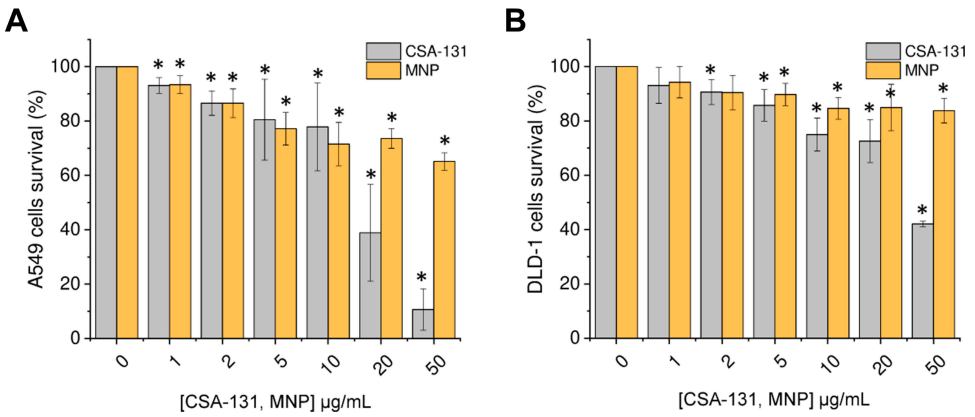

Figure 1 Cytotoxicity of ceragenin CSA-131 and magnetic nanoparticles (MNP) against lung carcinoma A549 and colon cancer DLD-1 cells. Decrease of lung cancer A549 (**A**) and colon cancer DLD-1 (**B**) cell viability after 24 hour treatment with ceragenin CSA-131 (grey bars) and MNP (yellow bars) in concentrations ranging from 1 to 50 µg/mL. Results are presented as mean ± SD from 3 to 6 individual experiments. *Indicates statistical significance (p-value < 0.05) when comparing to untreated control cells (0 µg/mL).

analyses were performed using Statistica 10 (StatSoft Inc, Tulsa, OK, USA), and $p<0.05$ was considered to be statistically significant.

Results

Lung and Colon Cancer Cells Treated with CSA-131 and MNP Exhibit Decrease in Cell Viability

To test whether ceragenin CSA-131 and iron oxide-based magnetic nanoparticles reduce lung and colon cancer cell viability, lung carcinoma A549 and colon cancer DLD-1 cells were incubated with increasing concentrations of test agents (concentrations ranging from 1 to 50 µg/mL) for 24 h. As shown in Figure 1 and Tables 1 and 2, treatment of both cancerous cell lines with CSA-131 resulted in a dose-dependent decrease of cell survival; at the highest tested dose, ie 50 µg/mL, cell growth of A549 and DLD-1 cells was inhibited by 89.34 ± 7.65% and 57.91 ± 1.03%, respectively. Using Chou-Talalay median-effect analyses, effective doses (ED) necessary to decrease the cellular viability by 10%, 50% and 75% were calculated by extrapolation from each dose-response curves; accordingly, ED10%, ED50% and ED75% were 2.03 ± 0.71, 12.63 ± 5.44 and 31.65 ± 14.89 µg/mL for A549 cells and 3.49 ± 3.45, 24.83 ± 5.69 and 201.4 ± 102.67 µg/mL for DLD-1 cells. Cancer cells were considerably less sensitive to MNP-mediated treatment (with no CSA-131), since at the dose of 50 µg/mL cell growth inhibition was 34.87 ± 3.22% and 16.18 ± 4.57% for lung and colon cancer cells, respectively.

Synthesis and Physicochemical Analysis of Ceragenin-Containing Nanoformulations

Given the 1) considerable anticancer potential of ceragenin CSA-131, 2) decrease of cancer viability upon MNP treatment and 3) previous reports on the intensification of antineoplastic features of biologically active compounds by nanomaterials, two questions were raised: (a) do ceragenin

Table 1 Relative Inhibitory Effects (RIE) of CSA-131, MNP@CSA-131 and CSA-131 + MNP on Lung Carcinoma A549 Cells Growth

(µg/mL)	CSA-131	MNP@CSA-131		CSA-131 + MNP	
	Cell Growth Inhibition (%)	Cell Growth Inhibition (%)	Relative Inhibitory Effect (%)	Cell Growth Inhibition (%)	Relative Inhibitory Effect (%)
1	6.92 ± 2.89	20.77 ± 15.93	+ 13.86 ± 13.05	13.91 ± 7.26	+ 7.00 ± 4.37
2	13.42 ± 4.47	31.54 ± 14.67	+ 18.12 ± 10.20	35.75 ± 3.40	+ 22.32 ± 1.07
5	19.48 ± 14.88	66.37 ± 4.09	+ 46.89 ± 10.79	54.88 ± 5.09	+ 35.40 ± 9.79
10	22.16 ± 16.16	98.23 ± 0.86	+ 76.07 ± 15.30	66.05 ± 2.61	+ 43.89 ± 13.59
20	61.13 ± 17.79	100.06 ± 0.55	+ 38.93 ± 17.24	92.87 ± 0.26	+ 31.74 ± 17.53
50	89.34 ± 7.65	100.06 ± 0.29	+ 10.72 ± 7.35	97.42 ± 1.01	+ 8.07 ± 6.63

Table 2 Relative Inhibitory Effects (RIE) of CSA-131, MNP@CSA-131 and CSA-131 + MNP on Colon Cancer DLD-1 Cells Growth

(μg/mL)	CSA-131	MNP@CSA-131		CSA-131 + MNP	
	Cell Growth Inhibition (%)	Cell Growth Inhibition (%)	Relative Inhibitory Effect (%)	Cell Growth Inhibition (%)	Relative Inhibitory Effect (%)
1	6.91 ± 6.62	8.28 ± 1.90	+ 1.37 ± 4.72	7.63 ± 3.30	+ 0.73 ± 3.32
2	9.35 ± 4.65	14.57 ± 5.79	+ 5.22 ± 1.15	13.66 ± 2.24	+ 4.31 ± 2.41
5	14.26 ± 5.86	26.76 ± 4.00	+ 12.49 ± 1.85	16.29 ± 3.25	+ 2.03 ± 2.61
10	25.01 ± 6.07	39.82 ± 13.18	+ 14.81 ± 7.11	35.09 ± 6.25	+ 10.08 ± 0.18
20	27.39 ± 7.92	45.93 ± 6.72	+ 18.55 ± 1.20	60.80 ± 2.75	+ 33.41 ± 5.17
50	57.91 ± 1.03	72.97 ± 1.80	+ 15.06 ± 0.78	80.87 ± 0.92	+ 22.96 ± 0.10

CSA-131 and MNP interact synergistically against tested cancer cell lines and (b) how this effect will be varied if ceragenin CSA-131 is covalently attached on the surface of MNP (MNP@CSA-131) or combined in one nanomixture (CSA-131+MNP). In one approach, CSA-131 was mixed with magnetic nanoparticles in 1:1 ratio, suspended in phosphate-buffered saline (PBS) and left for 48 h. In the second approach, a novel ceragenin-containing nanosystem was synthetized through glutaraldehyde and thoroughly analyzed.

FT-IR spectroscopy indicated that ceragenin CSA-131 was successfully attached to the nanoparticles surface via imine bonds (Figure 2A). The presence of iron oxide magnetic cores was confirmed by the intense band at 550 cm^{-1}, which corresponds to the Fe-O stretching mode of magnetite (Fe_3O_4). In the spectra of MNP and MNP@CSA-131, the extensive band at ~1000–1150 cm^{-1} might be ascribed to the stretching vibrations of organosilane derivatives such as Si-O-Si, Si-O, and Si-O-Fe. However, in the system containing CSA-131, more intense and wider signal was observed. The absorption peak at 1630 cm^{-1} was detected in the spectrum of the ceragenin-functionalized particles and was assigned to C=N stretching vibrations. Weak bands observed at 2853 and 2928 cm^{-1} were ascribed to C-H stretching modes. The signals above 3300 cm^{-1} were characterized as N-H stretching vibrations. Differential scanning calorimetry and thermogravimetric analysis were used to evaluate the thermal characteristic of synthesized nanosystems and support the data from FT-IR analysis. The DSC curves of analyzed nanoparticles (MNP and MNP@CSA-131, Figure 2B) indicate differences in the chemical nature of the coating. A new endothermic transition above 350°C is observed in the heating curve of CSA-131-modified particles. It is most likely associated with the presence of ceragenin and its partial decomposition. Figure 2C and D show thermogravimetric analysis results for MNP and MNP@CSA-131. TG and DTG data for CSA-131 are enclosed in Supplementary Material. A greater total weight loss of the MNP@CSA-131 compared to the MNP indicates successful functionalization.

Combined Therapy with Use of CSA-131-Containing Nanoformulations Exerts Enhanced Anticancer Activity When Compared to Single Treatments

The effect of combined treatment using CSA-131 and MNPs on lung and colon cancer cell viability was determined using the MTT assay. For this purpose, lung adenocarcinoma A549 and colon cancer DLD-1 cells were treated with MNP@CSA-131 and CSA-131+MNP at doses ranging from 1 to 50μg/mL and combination effects are summarized in Figure 3A and C. Combined treatment using MNP@CSA-131 and CSA-131 + MNP shifted the dose–response curves to lower doses indicating that activity of above compounds was greater than either CSA-131 or MNP alone. A considerable alteration in cytomorphological characteristics of A549 and DLD-1 cells were observed by inverted phase-contrast microscopy (Figure 3B and D). Compared to control cells, both treated lung and colon cancer cells, upon treatment with tested compounds, became less adhered, more round and shrunken, displaying vacuolization in cytoplasm. Importantly, these changes became progressively more pronounced when a combined treatment using CSA-131 and MNP was used.

Nevertheless, it is difficult to draw conclusions on a synergistic interaction between CSA-131 and MNP based on microscopic observations and dose–response

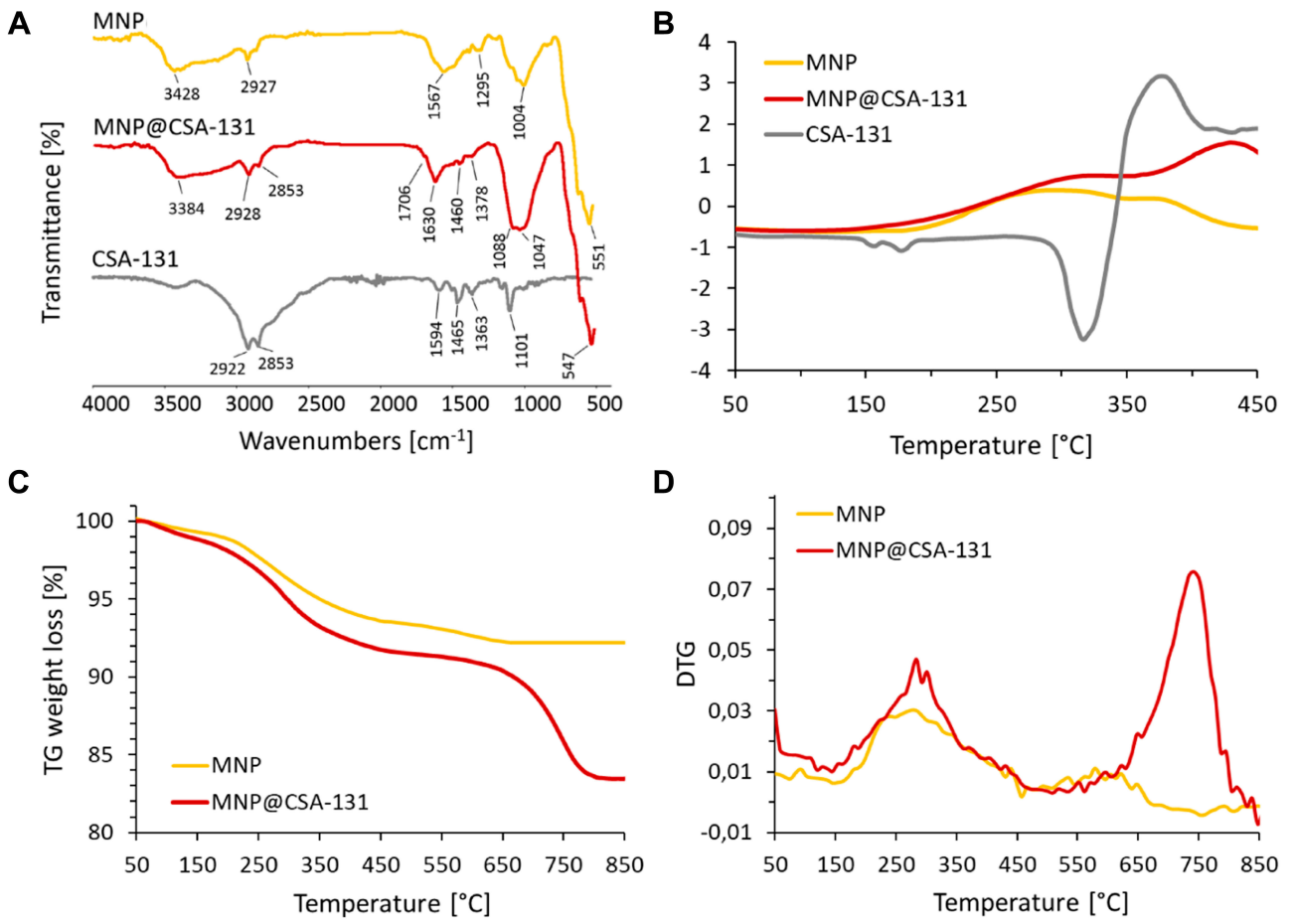

Figure 2 Physicochemical analysis of ceragenin CSA-131, ceragenin-containing nanosystem, MNP@CSA-131 and magnetic nanoparticles MNP. ATR FT-IR spectra of CSA-131 (grey curve), MNP@CSA-131 (red curve) and MNP (yellow curve) (**A**). Results of DSC, TGA and DTG analyses are presented in (**B–D**), respectively. TG and DTG data for CSA-131 are enclosed in Supplementary Materials.

curves alone, despite the statistically significant shifts. To more quantitively analyze the interactions between test compounds, relative inhibitory effect (RIE), combinatory index (CI) and dose reduction (DRI) values were calculated using the median effect principle method developed by Chau and Talalay.[29] The results of this analysis are summarized in Tables 1–4. Notably, combined treatment using CSA-131 with MNP exhibited synergistic interactions at all tested doses, since relative inhibitory effect (RIE) values were positive in a range from +0.73 ± 3.32% (for 1 µg/mL of CSA-131 + MNP against DLD-1 cells; Table 2) to +76.07 ± 15.30% (for 10 µg/mL of MNP@CSA-131 against A549 cell line; Table 1). More precisely, when comparing RIE values for both cells lines, it seems that covalent immobilization of CSA-131 on the surface of nanocarriers is more prone to exert synergistic effect – employment of combined treatment using MNP@CSA-131 intensify the activity of CSA-131 by 34.09% and 24.70% by average against A549 and DLD-1 cells, respectively. At the same time, a mixture of CSA-131+MNP improves the therapeutic efficiency of CSA-131 against A549 and DLD-1 cells by 11.25% and 12.52%, respectively (Tables 1 and 2). Accordingly, combined treatments resulted also in the decrease of effective doses (ED) values. As shown in Figure 4A and D, effective doses at 10%, 50% and 75% effects levels were 2.97 to 9.01-fold lower than those noted for a single treatment with CSA-131. These results indicated that the combination treatment was more powerful in decreasing both A549 and DLD-1 cell viability.

From the date described above, the combinatory index (CI) analysis demonstrated synergistic interactions between CSA-131 and MNP (Tables 3 and 4). Because our aim was to achieve maximal effects of tested nanoformulations, a mean combinatory index value was calculated for each tested dose and for each fraction affected (Fa) value (ie indicating the fraction of cells inhibited after drug exposure). To indicate the effects of drugs at different

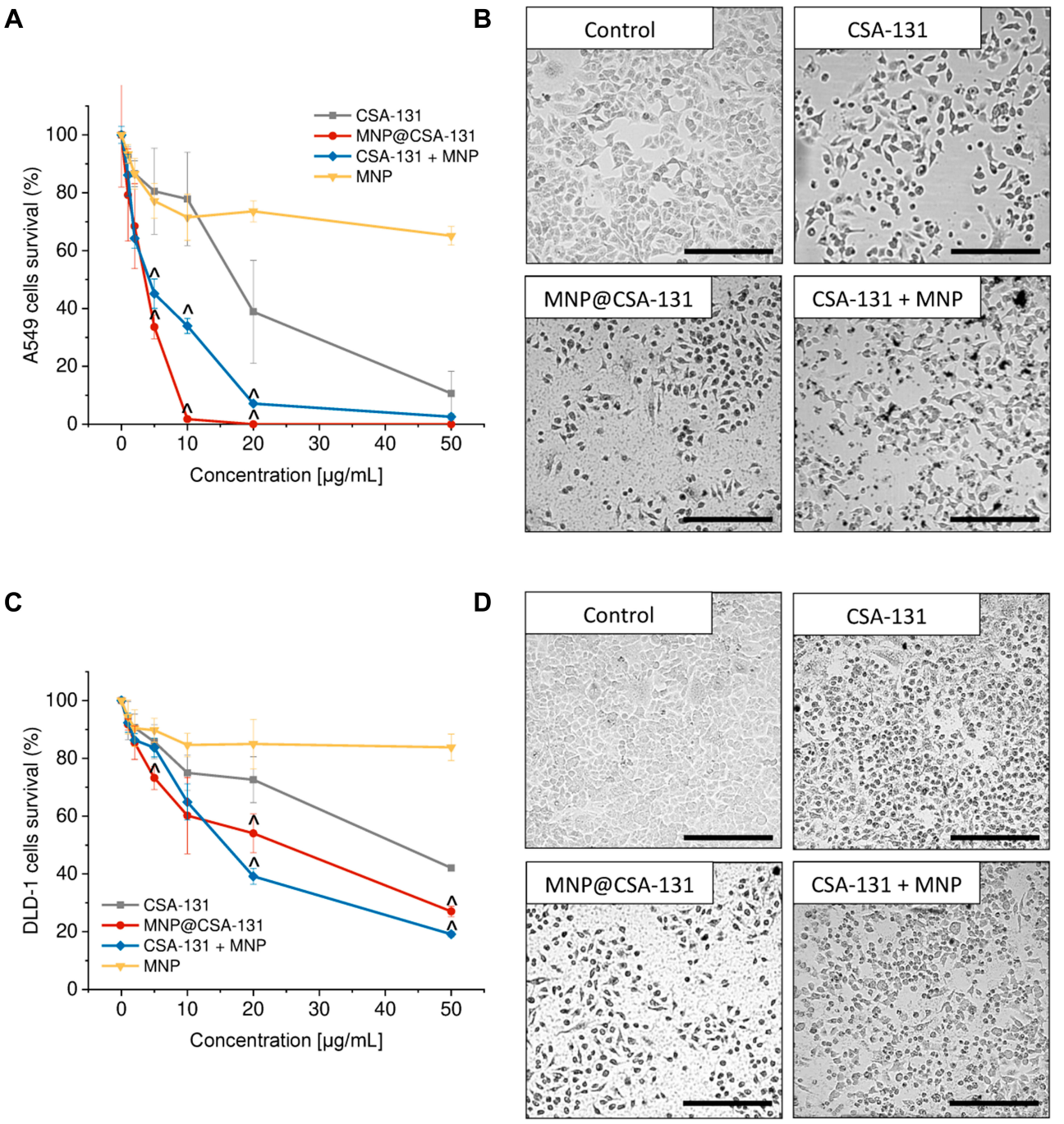

Figure 3 Cytotoxicity of ceragenin-containing nanocomposites against lung carcinoma A549 and colon cancer DLD-1 cells. Decrease of cancer cells viability and alterations in morphological features of lung (**A** and **B**, respectively) and colon cancer cells (**C** and **D**, respectively). For assessment of cytotoxicity, cells were treated for 24 hour with ceragenin CSA-131 (grey squares), MNP@CSA-131 (red circles), CSA-131 + MNP (blue diamonds) and MNP (yellow inverted triangles). Results are presented as mean ± SD from 3 to 6 individual experiments. ^Indicates statistical significance (*p*-value <0.05) when comparing to CSA-131-treated cells. Morphology of cancer cells were investigated upon treatment with 10 µg/mL of tested agents. Results from one representative experiment are shown. Black scale bar ~300 µm.

Fa values, Fa-CI plots were constructed (Figure 4B and E). As presented, non-beneficial interactions between ceragenin CSA-131 and MNPs were observed only for the lowest doses of MNP@CSA-131 and CSA-131+MNPs in the DLD1-based model, where Fa was less than 0.2. Considering that Fa <0.2 indicates low growth inhibition and a large population of cells actively growing, we considered these effects as less important than those at higher growth inhibition. For Fa > 0.6, CI values were below 1 indicating synergistic to mostly strong synergistic interactions. In addition, CI values of <1 corresponded to favorable DRI values (>1). According to the established

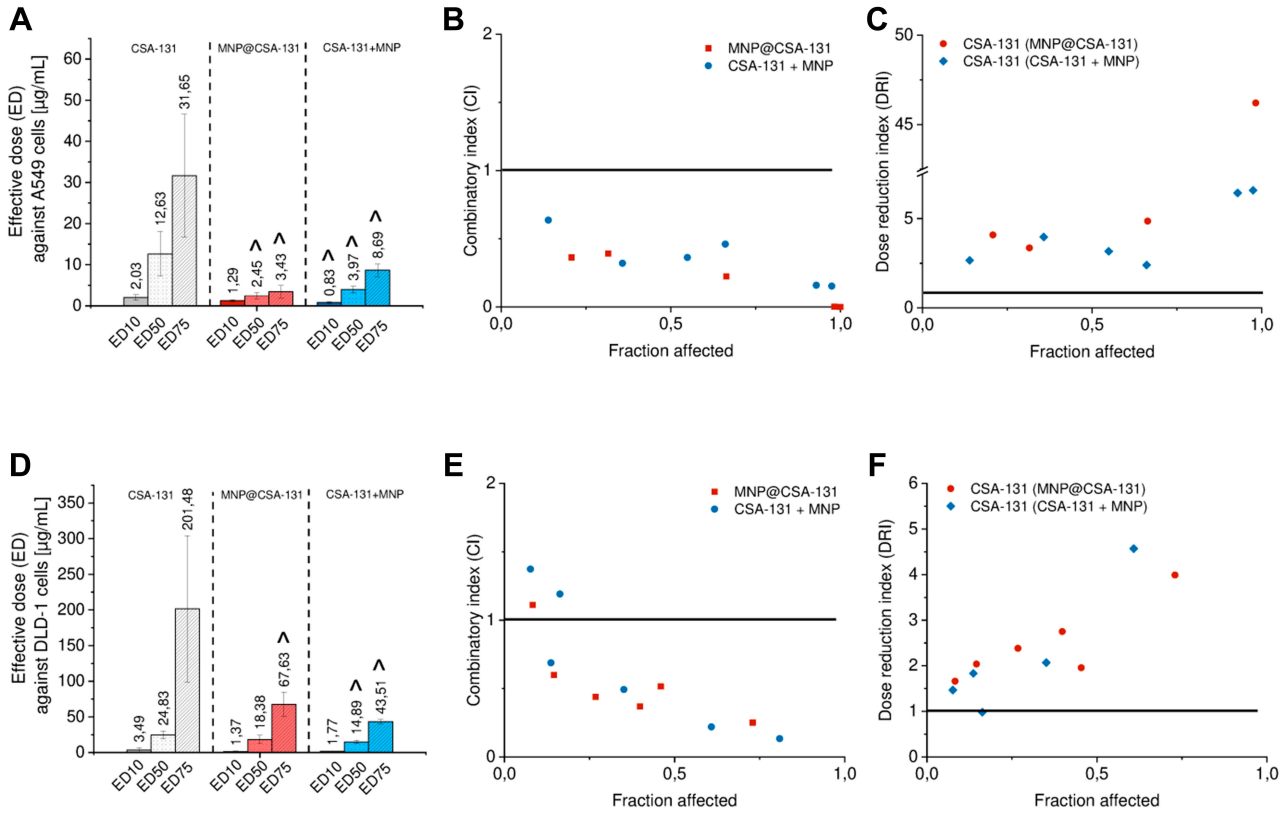

Figure 4 Effects of combined treatment of lung (**A**–**C**) and colon cancer cells (**D**–**F**) with ceragenin CSA-131 and magnetic nanoparticles. Effective doses at 10%, 50% and 75% effect levels of ceragenin CSA-131, MNP@CSA-131 and CSA-131 + MNP in lung cancer and colon cancer cells (**A** and **D**, respectively) calculated with Compusyn software from dose–response curves. Results are presented as mean ± SD from 3 to 6 individual experiments. ^Indicates statistical significance (p-value <0.05) when comparing to the effectiveness of CSA-131 alone. Illustrative Fa-CI (**B** and **E** for A549 and DLD-1 cell line, respectively) and Fa-DRI plots (**C** and **F** for A549 and DLD-1 cell lines, respectively). Data points represent the mean value calculated from triplicate experiments. Combinatory index (CI) and dose–response index (DRI) equal to 1 (indicated as black line on the plots) point out the additive effect and no dose reduction for combinatory treatment, respectively.

definition, DRI designates how many folds of dose reduction are allowed for each drug at a given effect level compared with the drug alone. Regardless of the dose and the cell line used, the DRI values were always >1, indicating a beneficial dose reduction of CSA-131. The Fa-DRI plots (Figure 4C and F) constructed using DRI for each Fa, indicate that chemotherapeutic doses of CSA-131 might be reduced from 1.17 ± 0.61 to 34.57 ± 12.78 times, which not only highlights the high capability of MNP to reduce effective doses of agents incorporated into nanoformulations, but most importantly, provides the possibility to improve the safety of performed cytostatic therapy.

Apoptosis Increases Death-Associated Effects in Cancer Cells Upon Combined Treatment Using CSA-131-Containing Nanoformulations

To more qualitatively describe the potential of combined treatment consisting of ceragenin CSA-131 and MNP, using covalent-based immobilization technique and co-treatment using both agents, a set of flow cytometry experiments was performed, and results of these studies are demonstrated in Figures 5 and 6. Due to the different content of ceragenin in the analyzed formulations, we decided to unify the tested amount and one dose of the substance was used for all combinations to compare the anti-cancer effects. Having in mind the dose-dependent toxicity of ceragenin against mammalian cells, flow cytometry analyses were carried out at a dose of 10 µg/mL. Increased levels of reduced glutathione (GSH) in ceragenin-treated cancer cells were observed, which indicates the introduction of cells into death processes (Figures 5A and 6A), conditioned by the exhaustion of intracellular reductive substances and rapid oxidative stress in treated cells. When compared to untreated, control cells characterized by the relatively low level of GSH (16.25 ± 11.24% and 23.5 ± 3.54% for A549 and DLD-1 cells, respectively), treatment of cancer cells with ceragenin CSA-131 resulted in a nearly 3-fold increase

Table 3 Analysis of the Combinatory Index (CI) and Dose-Reduction (DRI) of MNP@CSA-131 and CSA-131 + MNP Against Lung Carcinoma A549 Cells

(μg/mL)	MNP@CSA-131			CSA-131 + MNP		
	CI	Effect	DRI	CI	Effect	DRI
1	0.30 ± 0.09	S	3.39 ± 1.69	0.41 ± 0.32	S	12.29 ± 16.70
2	0.50 ± 0.24	S	2.92 ± 0.54	0.34 ± 0.08	S	3.74 ± 1.15
5	0.27 ± 0.10	SS	4.28 ± 1.48	0.41 ± 0.12	S	2.84 ± 0.88
10	0.03 ± 0.01	SS	34.57 ± 12.78	0.56 ± 0.24	S	2.14 ± 0.83
20	0.004 ± 0.01	SS	>100*	0.24 ± 0.17	SS	5.37 ± 2.7
50	0.006 ± 0.01	SS	>100*	0.23 ± 0.11	SS	4.99 ± 1.96

Notes: Combinatory index (CI) values >1 indicate antagonistic effect (AN); CI = 1 indicates additive effect (A); values between 1 and 0.76 indicate slight synergistic effects (SIS); values <0.75–0.3 indicate synergy (S) and <0.3 indicate strong synergistic effect (SS). Dose-reduction index (DRI) values >1 indicate favorable dose reduction, DRI<1 indicate unfavorable dose reduction, DRI=1 indicate no dose reduction. *Indicate values with low level of certainty in a dose range tested.

Table 4 Analysis of the Combinatory Index (CI) of MNP@CSA-131 and CSA-131 + MNP Against Colon Cancer DLD-1 Cells

(μg/mL)	MNP@CSA-131			CSA-131 + MNP		
	CI	Effect	DRI	CI	Effect	DRI
1	1.38 ± 0.25	AN	2.55 ± 2.27	3.50 ± 3.47	AN	2.08 ± 1.48
2	1.02 ± 0.35	A	2.39 ± 0.80	1.11 ± 0.62	AN	2.35 ± 1.59
5	0.51 ± 0.17	S	2.47 ± 0.56	1.58 ± 0.55	AN	1.17 ± 0.61
10	0.47 ± 0.11	S	3.20 ± 1.68	0.60 ± 0.14	S	2.07 ± 0.13
20	0.73 ± 0.21	S	1.94 ± 0.55	0.43 ± 0.21	S	4.16 ± 1.56
50	0.69 ± 0.45	S	3.70 ± 2.06	0.51 ± 0.41	S	7.10 ± 4.76

Notes: Combinatory index (CI) values >1 indicate antagonistic effect (AN); CI = 1 indicates additive effect (A); values between 1 and 0.76 indicate slight synergistic effects (SIS); values <0.75–0.3 indicate synergy (S) and <0.3 indicate strong synergistic effect (SS). Dose-reduction index (DRI) values >1 indicate favorable dose reduction, DRI<1 indicate unfavorable dose reduction, DRI=1 indicate no dose reduction.

of reduced GSH, confirming the anti-cancer potential of this compound against lung and colon carcinomas. More importantly, this effect was further intensified when cells were exposed to MNP@CSA-131 or CSA-131 + MNP in doses corresponding to ceragenin concentrations. This observation was confirmed by the introduction of cells into orange acridine (AO)/propidium iodide (PI) double staining, which allowed for discrimination between 1) viable, healthy cells, 2) PI-negative cells with low viability and 3) PI-positive dead cells with permeable membranes. According to results shown in Figures 5B and 6B, both MNP@CSA-131 and CSA-131+MNP in a dose of 10 μg/mL significantly increased the number of dead and membrane-permeable cells – combined treatment induced killing processes in extra 30.8% and 20.9% of A549 and DLD-1 cells, respectively, when compared to CSA-131 alone. This observation was also confirmed by resazurin-based quantification of the ability of treated cancer cells to proliferate – as shown in Figures 5C and 6C. Tested agents efficiently arrested the proliferation of nanoformulation-treated cells, with MNP@CSA-131 as the most effective agent.

To investigate the killing mechanism of ceragenin CSA-131 and ceragenin-containing nanoformulations, the externalization of phosphatidylserine (PS) into the outer leaflet of cell membranes was investigated using FITC-labeled Annexin V followed by PI-staining of cells (apoptosis assay). As shown in Figures 5D and 6D, combined treatment with CSA-131 + MNP increased the level of late apoptotic cells to 68.68 ± 8.88% and 52.76 ± 3.29% for A549 and DLD-1 cells, respectively. At the same time, the number of necrotic cells remained unchanged when compared to control and CSA-131-treated cells, which indicates that the killing ability of these compounds is determined by the induction of apoptosis processes. This observation is also in agreement with fluorescence microscopic observations of genetic material destruction upon exposed treatment (Figures 5E and 6E). Considering that DNA fragmentation is recognized as a major and most crucial event occurring in late apoptosis, it is justified to state that ceragenin-containing nanoformulations do not alter the route of cells death, but only intensify the main killing ceragenin-associated mechanisms.

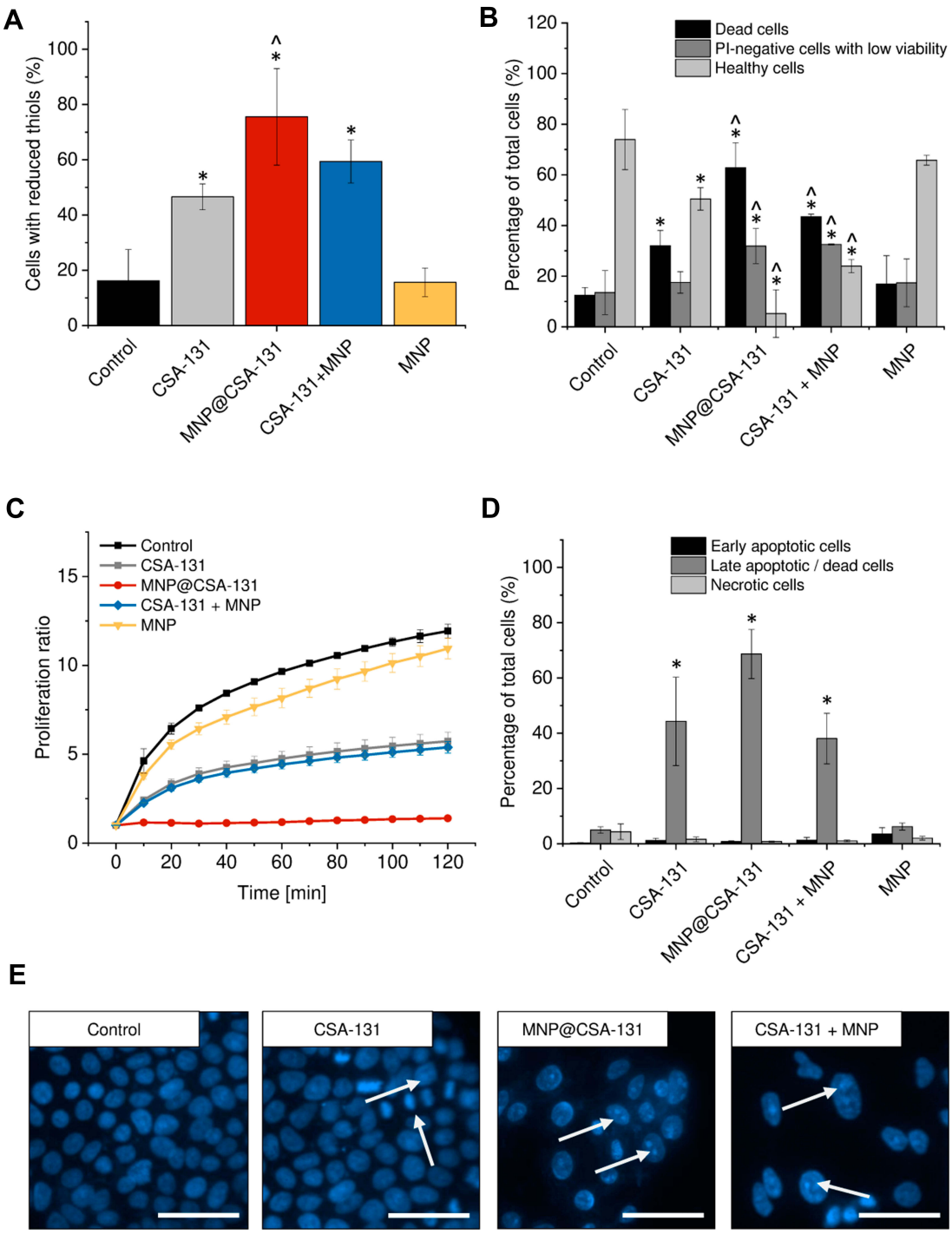

Figure 5 Anticancer activity of ceragenin CSA-131 and ceragenin-containing nanoformulations against lung carcinoma A549 cells. Increase of intracellular levels of reduced thiols in A549 cells treated with CSA-131 (grey bar), MNP@CSA-131 (red bar), CSA-131+MNP (blue bar) and MNP (yellow bar) when compared to untreated control (0 μg/mL; black bar) (**A**). The percentages of dead cells (black columns), PI-negative cells with low viability (dark grey columns) and healthy cells (light grey columns) in lung carcinoma cells treated with CSA-131, MNP@CSA-131, CSA-131 and MNP or naked MNPs (**B**). The proliferation of cancer cells treated with CSA-131 (grey squares), MNP@CSA-131 (red circles), CSA-131 + MNP (blue diamonds) and MNP (yellow inverted triangles) when compared to untreated control (black squares) estimated using resazurin-based fluorimetric method (**C**). Induction of apoptosis in A549 cells by CSA-131 and its magnetic derivatives (**D**). Percentage of early apoptotic (black columns), late apoptotic/dead cells (dark grey columns) and dead cells (light grey columns). For the purpose of the clarity of the presented data, live cells (Annexin V-negative and 7-AAD-negative) were not presented in the provided figures. Morphological alternations in nuclei of A549 cells upon treatment with CSA-131, MNP@CSA-131 and CSA-131 + MNP when compared to uncreated cells (**E**). White arrows indicate treatment-induced morphological changes in nuclei of treated cells. All experiments were performed using agents at a concentration of 10 μg/mL for 24 h. (**A**–**D**) demonstrate results from 3 to 6 individual experiments ± SD, for panel E results from one representative experiment are shown. * and ^ indicate statistical significance (*p*-value <0.05) when comparing to control cells (0 μg/mL) and CSA131-treated cells, respectively. Scale bar ~50 μm.

CSA-131 in Combination with Magnetic Nanoparticles Improves the Hemocompatibility and Membrane-Permeabilizing Properties

A considerable limitation in the clinical introduction of membrane-active compounds with anticancer activity is their low selectivity and thus, potential damage to host cells membranes. To evaluate whether combining of ceragenin CSA-131 in MNP-based nanoformulations would prevent toxic effects against host cells, a hemolysis assay was performed. In this assay, isolated red blood cells act as a model of host membranes, allowing for the determination of membrane-permeabilizing properties of designed agents. As presented in Figure 7, ceragenin-based nanosystems are characterized by low hemolytic activity in a broad spectrum of doses, up to 50 μg/mL, ie doses 5 times higher than effective against cancer cells. At dose of 20 μg/mL MNP@CSA-131 and CSA-131+MNP induce hemoglobin release from only 3.07 ± 3.57% and 1.47 ± 0.79% red blood cells, when CSA-131 alone damage 34.04 ± 10.12% of RBCs at the same dose. Using dose–response curves, MHC10% (minimal hemolytic concentration causing the release of hemoglobin from 10% red blood cells) was calculated. Importantly, MHC10% for MNP@CSA-131 and CSA-131+MNP were 7.88 and 4.72-fold higher than for CSA-131 alone, clearly indicating the improvement of hemocompatibility of ceragenin CSA-131 upon its immobilization with magnetic nanoparticles.

Discussion

Currently, a variety of both single and combinatory therapies is proposed as an option for the treatment of lung adenocarcinoma and colon cancer; nevertheless, high numbers of drug-resistant tumors and considerable toxicity of currently used chemotherapeutics hamper the treatment process.[31,32] Efforts are being made to design potent cytostatics characterized by lower toxicity. Ceragenins, due to their favorable pharmacodynamic features and nonspecific, cellular membrane-based mechanism of action, are currently tested as potential anticancer agents.[4–6,33] Previous reports have demonstrated that ceragenin CSA-13 effectively inhibits the proliferation capability of cancer cells in vitro and disrupt the oxidative balance of treated cells resulting in the induction of apoptosis.[4,5] Nevertheless, in higher doses of ceragenins of approx. 50–100 μg/mL, considerable hemolysis and cellular toxicity are observed, restricting its utility via intravascular routes.[7] Responding to the basic assumptions of combined therapy, we aimed to create a ceragenin-containing nanoformulation with high anticancer activity and low toxicity at the same time, which is easy to synthetize and cost-effective. To date, a variety of nanomaterials, including liposomes,[34] polymeric nanoparticles,[35] dendrimers,[36] carbon nanoparticles[37] and metallic nanoparticles[38] were demonstrated as compounds enhancing the anticancer effectiveness of conventional chemotherapeutics. In our study, the employment of iron oxide-based magnetic nanoparticles as synergistic agents in combination with ceragenin CSA-131 was encouraged and justified by our previously published reports, clearly indicating the improvement of activity of ceragenins, particularly ceragenin CSA-13, in the presence of magnetic nanoparticles.[7,24,30,39] Apart from the role of MNP as drug nano-delivers, we believe that a significant advantage of magnetic nanoparticles employment when compared to other materials is the possibility to easily purify developed nanosystems from residues of reagents that are necessary for the proper functionalization of anticancer drugs and relatively low toxicity of MNP. A compelling number of studies indicate that aminosilane coating reduces the toxicity of iron oxide nanoparticles,[23] making them appropriate agents for combining with other anticancer agents. Considering the above assumptions, we have chosen a relatively low concentration of CSA-131 (10 μg/mL) in combination with magnetic nanoparticles, both covalently attached or co-administrated together in one nanomixture to explore the synergistic inhibitory effect against lung A549 adenocarcinoma and colon DLD-1 cancer cells. When assessing cell growth inhibition, we have noted that for clinically relevant cytotoxicity, higher doses of tested agents, particularly magnetic nanoparticles, are required (Figure 1). At the same time, combinations of these therapeutics have demonstrated significant synergy and dose-reduction effects, which suggest that the combined use of MNPs could strongly limit the toxicity of ceragenin CSA-131 by reducing its effective dose (Figure 4, Tables 3 and 4). Although a majority of studies aiming to assess the improvement of killing abilities of ceragenins using MNP involve covalent-based nanosystems, it was demonstrated that antibacterial properties of membrane-active compounds against *Pseudomonas aeruginosa* and *Staphylococcus aureus* might be potentiated by combining the ceragenin with aminosilane-, gold- or poly (quaternary ammonium salt-coated iron oxide nanoparticles).[24] Anticancer activities of those formulations and mathematic quantification of such have not been investigated to date, which highlights the novelty of this research. According to our results, both MNP@CSA-131 and CSA-131 +MNP nanoformulations exert accelerated inhibitory effects.

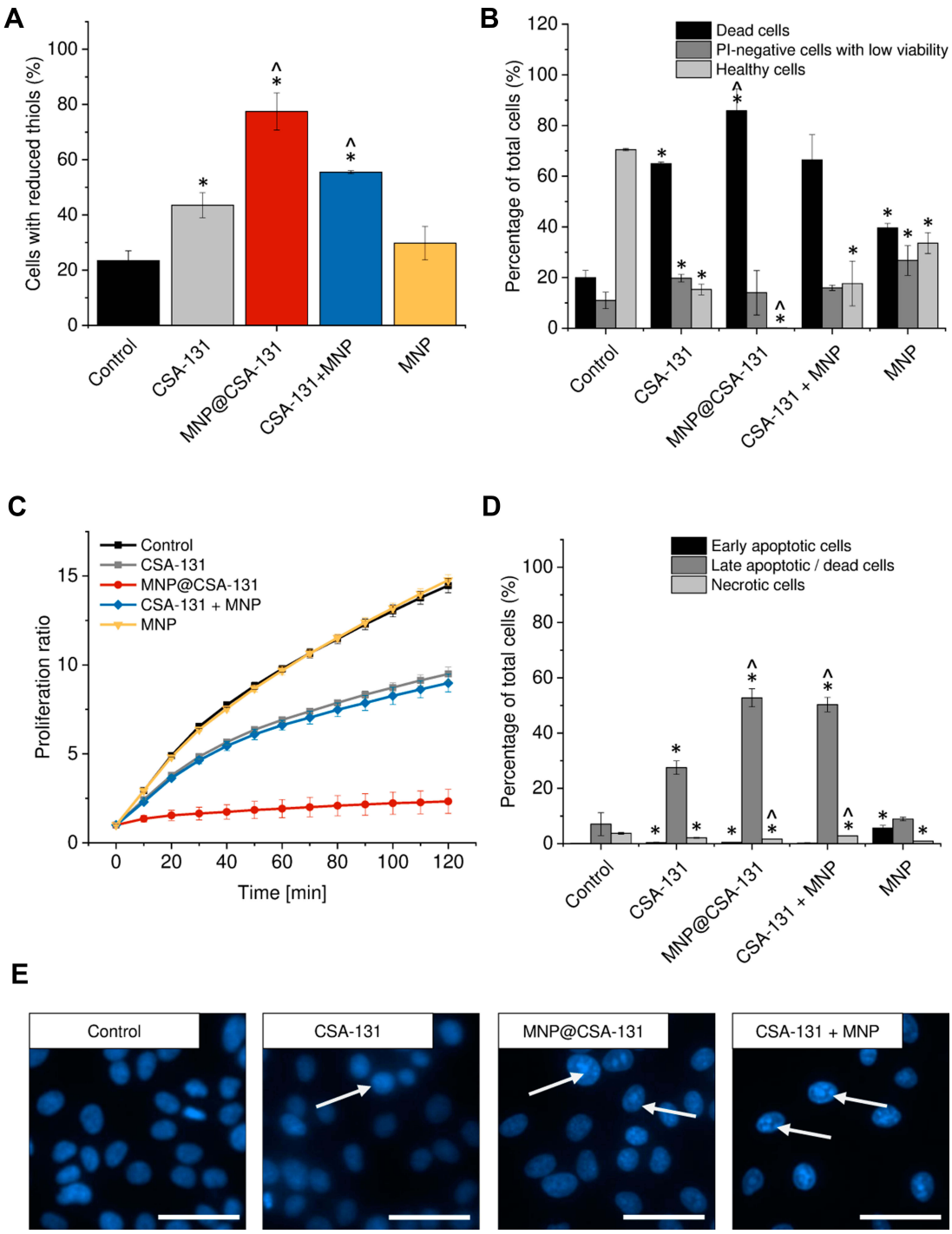

Figure 6 Anti-cancer activity of ceragenin CSA-131 and ceragenin-containing nanoformulations against colon cancer DLD-1 cells. Increase of intracellular levels of reduced thiols in DLD-1 cells treated with CSA-131 (grey bar), MNP@CSA-131 (red bar), CSA-131+MNP (blue bar) and MNP (yellow bar) when compared to untreated control (0 μg/mL; black bar) (**A**). The percentages of dead cells (black columns), PI-negative cells with low viability (dark grey columns) and healthy cells (light grey columns) in colon carcinoma cells treated with CSA-131, MNP@CSA-131, CSA-131 and MNP or naked MNPs (**B**). The proliferation of cancer cells treated with CSA-131 (grey squares), MNP@CSA-131 (red circles), CSA-131 + MNP (blue diamonds) and MNP (yellow inverted triangles) when compared to untreated control (black squares) estimated using resazurin-based fluorimetric method (**C**). Induction of apoptosis in DLD-1 cells by CSA-131 and its magnetic derivatives (**D**). Percentage of early apoptotic (black columns), late apoptotic/dead cells (dark grey columns) and dead cells (light grey columns). For the purpose of the clarity of the presented data, live cells (Annexin V-negative and 7-AAD-negative) were not presented in the provided figures. Morphological alternations in nuclei of DLD-1 cells upon treatment with CSA-131, MNP@CSA-131 and CSA-131 + MNP when compared to uncreated cells (**E**). White arrows indicate treatment-induced morphological changes in nuclei of treated cells. All experiments were performed using agents at a concentration of 10 μg/mL for 24 h. (**A**–**D**) demonstrate results from 3 to 6 individual experiments ± SD, for (**E**) results from one representative experiment are shown. * and ^ indicate statistical significance (p-value <0.05) when comparing to control cells (0 μg/mL) and CSA131-treated cells, respectively. Scale bar ~50 μm.

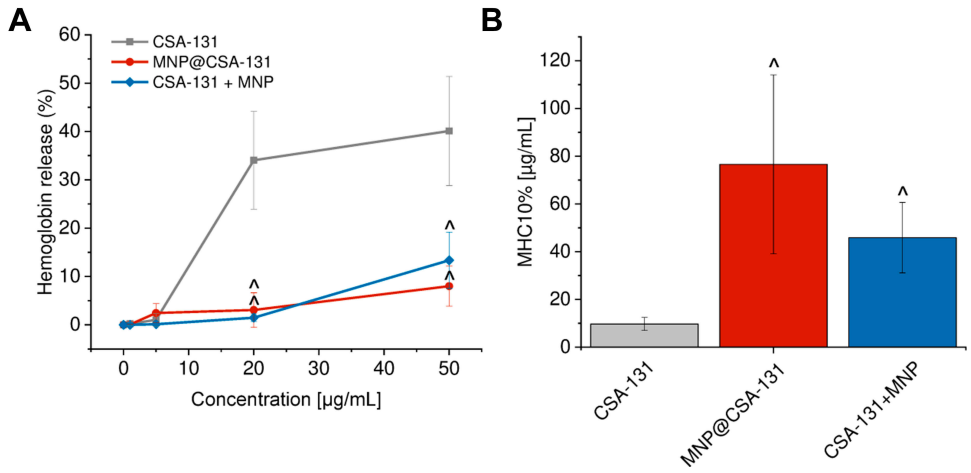

Figure 7 Improvement of hemocompatibility of ceragenin CSA-131 when attached to MNP surface. Hemoglobin released from red blood cells incubated in the presence of CSA-131 (grey squares), MNP@CSA-131 (red circles) and CSA-131+MNP (blue diamonds) at concentrations ranging from 0 to 50 µg/mL (**A**). Minimal concentrations of CSA-131 (grey bar), MNP@CSA-131 (red bar) and CSA-131+MNP (blue bar) required to induce hemolysis in 10% of RBCs (**B**). Results are presented as mean ± SD from 3 to 6 individual experiments. ^Indicates statistical significance (*p*-value <0.05) when comparing to CSA131-treated cells.

Although comparative analysis of these nanoagents is considerably hampered due to different amount of ceragenin in those formulations, a favorable interaction between MNP and CSA-131 is strongly highlighted in both cases, since the ED75 of MNP@CSA-131 was 2.97–9.22 fold lower and the ED75 of CSA-131+MNP was 3.64–4.62 fold lower when compared to free CSA-131 (Figure 4A and D). Analysis of combinatory effects using the Chou-Talalay method indicated mostly synergistic or strong synergistic interactions between tested compounds, highlighting their utility as nanoagents for lung and colon cancer treatment (Tables 3 and 4). These results suggest that not only covalent attachment of ceragenin CSA-131 to MNP surface but also simple combining of these agents into one nanomixture seems to be sufficient to exert potent anticancer activity, which provides new possibilities to design novel ceragenin-containing nanoformulations. Our data are in agreement with previous reports demonstrating the possibility to co-deliver antineoplastic agents using metal nanoparticles.[40,41] Most recently, Tao et al prepared novel disulfiram/doxorubicin co-loaded nanoparticles using the attraction of cytostatic to NPs. Accordingly, disulfiram and doxorubicin were found to have increased intracellular accumulation in breast cancer cells, compared to free drug solutions.[40] Synergistic effect of silver nanoparticles conjugated with gemcitabine against metastatic breast cancer cells resulted in a significant reduction of both gemcitabine and silver nanoparticles effective doses, and thus, has allowed for improvement of treatment safety.[41] Importantly, combining of active agents into one nanomixture as indicated by Karuppaiah et al were much simpler and cost-effective methods, when compared to linkers required for covalent immobilization.[41] We suggest that similar advantages might be recognized for ceragenin-containing nanoformulation proposed in this work. Although the exact mechanism of observed synergistic interactions was not determined in this study, some hypotheses can be made. Firstly, it is suggested that enhanced anticancer activity of developed nanoformulations results from the increased intracellular accumulation of CSA-131. Previous studies clearly indicated that iron oxide magnetic nanoparticles exert a synergistic effect with daunorubicin due to enhanced drug uptake of targeted leukemia cells.[42] Effective delivery of daunorubicin and let-7a mRNA on the surface of zinc-doped iron oxide core nanoparticles with mesoporous silica was demonstrated to be efficient to overcome drug-resistance in breast cancer cells.[43] Our previously published research performed using HT-29 colon cells revealed increased cellular internalization of MNP@CSA-13 when compared to free alone.[6] Although the similar analyses employing CSA and MNP simply combined were not performed to date, it is suggested that a similar mechanism might determine the therapeutic effectiveness of CSA-131+MNP. The second hypothesis, which does not exclude the mechanism proposed above, assumes that both MNP and CSA-131 target similar points in cancer cells resulting in an increase of overall cytotoxicity. Our previous study performed using breast cancer MCF-7 cells clearly indicated that ceragenin CSA-13 acts as pro-apoptotic agents due to the induction of excessive oxidative stress followed by membrane depolarization, caspases activation and DNA fragmentation and this effect is further intensified by attachment of CSA-13 to

MNP surface.[4] At the same time, Alarifi et al demonstrated that iron oxide nanoparticles attack mitochondria, which are redox-active organelles, leading to oxidative stress generation and cell death.[44] Based on the above data, it is hypothesized that the observed increased killing effect of MNP@CSA-131 and CSA-131+MNP results from increased CSA-131 uptake by lung and colon cancer cells and from the fact that both CSA-131 and MNP exert pro-apoptotic activities and this effect is only intensified when administrated simultaneously.

Properly planned and carried out synergistic therapy requires not only increases in the tumor response to the treatment used but also reduction of the initial toxicity and preventing its overlapping in the case of drugs with different mechanisms of action and chemical structure. In this work, due to the utility of ceragenin-decorated nanoformulations, we present the possibility of limiting the membrane-permeabilizing properties of CSA-131 and thus, to increase the safety of such treatments, even when systemically administered. Previous studies demonstrated that limitations of the membrane-damaging activity of ceragenin CSA-13 might be achieved by covalent immobilization of CSA-13 on the surface of iron oxide magnetic nanoparticles, resulting in a decrease of hemolysis from 40% to less than 1%.[7] In our current work, MNP-based nanoformulations were found to be non-hemolytic in effective, anticancer doses. As presented in Figure 7, up to a dose of 20 μg/mL, hemolysis did not exceed 2.5% when MNP@CSA-131 and CSA-131+MNP were tested, while unconjugated CSA-131 induced hemoglobin release in approx. 35% of red blood cells at the same concentration. These results confirm that both of the combined nanoformulations are sufficient to prevent erythrocytes damage. Therefore, improving the safety of ceragenin-containing nanoagents and understanding the key mechanisms governing this process are necessary to create optimal ceragenin-containing nanoformulations for medical applications. Some reports suggest that this effect can be determined by the stable immobilization of drugs on the nanomaterial surface as shown for daunorubicin encapsulated on self-assembled magnetic iron oxide nanoparticles.[45] While this mechanism is potentially involved in higher hemocompatibility of MNP@CSA-131, its effect on the toxicity of CSA-131+MNP remains unclear. Similar protective mechanism of silver nanoparticles (AgNPs) against hemolytic activities of membrane-permeabilizing antimicrobial peptides was demonstrated by Ruden et al.[46] Accordingly, the addition of increasing concentrations of AgNP caused a decrease in the hemolytic activity of PGLa peptide, magainin 2, gramicidin S, polymyxin B and gramicidin A, but this issue requires additional analysis.[46]

Our results suggest a promising approach for using a combination of ceragenin CSA-131 with iron oxide nanoparticles in the development of new cancer treatment. Nanoformulations explored in this study possess two important features: they are characterized by potent anticancer activity against colon and lung carcinoma cells and possess satisfactory hemocompatibility, and their lack of substantial hemolytic activity may allow for systemic administration. Our results suggest that the strategy to utilize iron oxide magnetic nanoparticles as a carrier of ceragenin CSA-131 might be a highly efficient approach to achieve anticancer synergism. This indicates new directions for the preparation of MNP-based drugs, which may be relatively easy to synthesize, cost-effective and safe when administered intravenously.

Ethics Statement

Hemolytic activity of tested agents was evaluated in blood samples from adult healthy volunteers under IRB approval: R-I-002/382/2012. This study was approved by the institutional review board (IRB) of The Medical University of Bialystok. The study was in accordance with the Declaration of Helsinki and written informed consent was provided by the blood donors.

Acknowledgments

The authors are grateful for Dr Izabela Prokop from the Department of Medicinal Chemistry, Medical University of Bialystok for assistance during microscopic analyses.

Funding

This work was financially supported by grants from the National Science Centre, Poland (UMO-2015/19/N/NZ6/01872 to EP) and Medical University of Bialystok (SUB/1/DN/19/001/1162 to RB). Part of the study was conducted with the use of equipment purchased by the Medical University of Białystok as part of the RPOWP 2007-2013 funding, Priority I, Axis 1.1, contract No. UDA- RPPD.01.01.00-20-001/15-00 dated 26.06.2015. The synthesis and physicochemical analysis of magnetic nanoparticles and MNP-based compounds were performed in the Centre of Synthesis and Analysis BioNanoTechno of the University of Bialystok (POPW.01.03.00-20-034/09-00 and POPW.01.03.00-20-004/11 projects). This work was supported by the program of the Minister of Science and Higher Education under the name “Regional Initiative of

Excellence in 2019-2022", project number: 024/RID/2018/19, financing amount: 11.999.000,00 PLN. The funders had no role in study design, data collection and analysis, decision to publish, or preparation of the manuscript.

Disclosure

PBS is a paid consultant for N8 Medical, Inc. All other authors declare that they have no competing interests.

References

1. Felício MR, Silva ON, Gonçalves S, Santos NC, Franco OL. Peptides with dual antimicrobial and anticancer activities. *Front Chem*. 2017;5:5. doi:10.3389/fchem.2017.00005
2. Deslouches B, Di YP. Antimicrobial peptides with selective antitumor mechanisms: prospect for anticancer applications. *Oncotarget*. 2017;8(28):46635–46651. doi:10.18632/oncotarget.16743
3. Baxter AA, Lay FT, Poon IKH, Kvansakul M, Hulett MD. Tumor cell membrane-targeting cationic antimicrobial peptides: novel insights into mechanisms of action and therapeutic prospects. *Cell Mol Life Sci*. 2017;74(20):3809–3825. doi:10.1007/s00018-017-2604-z
4. Piktel E, Prokop I, Wnorowska U, et al. Ceragenin CSA-13 as free molecules and attached to magnetic nanoparticle surfaces induce caspase-dependent apoptosis in human breast cancer cells via disruption of cell oxidative balance. *Oncotarget*. 2018;9(31):21904–21920. doi:10.18632/oncotarget.25105
5. Kuroda K, Fukuda T, Okumura K, et al. Ceragenin CSA-13 induces cell cycle arrest and antiproliferative effects in wild-type and p53 null mutant HCT116 colon cancer cells. *Anticancer Drugs*. 2013;24(8):826–834. doi:10.1097/CAD.0b013e3283634dd0
6. Niemirowicz K, Prokop I, Wilczewska AZ, et al. Magnetic nanoparticles enhance the anticancer activity of cathelicidin LL-37 peptide against colon cancer cells. *Int J Nanomedicine*. 2015;10:3843–3853. doi:10.2147/IJN.S76104
7. Niemirowicz K, Surel U, Wilczewska AZ, et al. Bactericidal activity and biocompatibility of ceragenin-coated magnetic nanoparticles. *J Nanobiotechnol*. 2015;13(1):32. doi:10.1186/s12951-015-0093-5
8. Navya PN, Kaphle A, Srinivas SP, Bhargava SK, Rotello VM, Daima HK. Current trends and challenges in cancer management and therapy using designer nanomaterials. *Nano Converg*. 2019;6(1):23.
9. Niemirowicz K, Markiewicz KH, Wilczewska AZ, Car H. Magnetic nanoparticles as new diagnostic tools in medicine. *Adv Med Sci*. 2012;57(2):196–207. doi:10.2478/v10039-012-0031-9
10. Tokajuk G, Niemirowicz K, Deptula P, et al. Use of magnetic nanoparticles as a drug delivery system to improve chlorhexidine antimicrobial activity. *Int J Nanomedicine*. 2017;12:7833–7846. doi:10.2147/IJN.S140661
11. Fathima JB, Pugazhendhi A, Venis R. Synthesis and characterization of ZrO. *Microb Pathog*. 2017;110:245–251. doi:10.1016/j.micpath.2017.06.039
12. Sathiyavimal S, Vasantharaj S, Bharathi D, et al. Biogenesis of copper oxide nanoparticles (CuONPs) using Sida acuta and their incorporation over cotton fabrics to prevent the pathogenicity of Gram negative and Gram positive bacteria. *J Photochem Photobiol B*. 2018;188:126–134. doi:10.1016/j.jphotobiol.2018.09.014
13. Pugazhendhi A, Prabhu R, Muruganantham K, Shanmuganathan R, Natarajan S. Anticancer, antimicrobial and photocatalytic activities of green synthesized magnesium oxide nanoparticles (MgONPs) using aqueous extract of Sargassum wightii. *J Photochem Photobiol B*. 2019;190:86–97. doi:10.1016/j.jphotobiol.2018.11.014
14. Chen Z, Zheng Y, Shi Y, Cui Z. Overcoming tumor cell chemoresistance using nanoparticles: lysosomes are beneficial for (stearoyl) gemcitabine-incorporated solid lipid nanoparticles. *Int J Nanomedicine*. 2018;13:319–336. doi:10.2147/IJN.S149196
15. Kouassi GK, Irudayaraj J. Magnetic and gold-coated magnetic nanoparticles as a DNA sensor. *Anal Chem*. 2006;78(10):3234–3241. doi:10.1021/ac051621j
16. Maddinedi SB. Green synthesis of Au–Cu2−xSe heterodimer nanoparticles and their in-vitro cytotoxicity, photothermal assay. *Environ Toxicol Pharmacol*. 2017;53:29–33. doi:10.1016/j.etap.2017.05.006
17. Maddinedi SB, Mandal BK, Anna KK. Tyrosine assisted size controlled synthesis of silver nanoparticles and their catalytic, in-vitro cytotoxicity evaluation. *Environ Toxicol Pharmacol*. 2017;51:23–29. doi:10.1016/j.etap.2017.02.020
18. Maddinedi SB, Mandal BK, Maddili SK. Biofabrication of size controllable silver nanoparticles - A green approach. *J Photochem Photobiol B*. 2017;167:236–241. doi:10.1016/j.jphotobiol.2017.01.003
19. Maddinedi SB, Mandal BK, Anna KK. Environment friendly approach for size controllable synthesis of biocompatible Silver nanoparticles using diastase. *Environ Toxicol Pharmacol*. 2017;49:131–136. doi:10.1016/j.etap.2016.11.019
20. Pugazhendhi A, Edison TNJI, Karuppusamy I, Kathirvel B. Inorganic nanoparticles: a potential cancer therapy for human welfare. *Int J Pharm*. 2018;539(1–2):104–111. doi:10.1016/j.ijpharm.2018.01.034
21. Vasantharaj S, Sathiyavimal S, Senthilkumar P, LewisOscar F, Pugazhendhi A. Biosynthesis of iron oxide nanoparticles using leaf extract of Ruellia tuberosa: antimicrobial properties and their applications in photocatalytic degradation. *J Photochem Photobiol B*. 2019;192:74–82. doi:10.1016/j.jphotobiol.2018.12.025
22. Jiang Z, Shan K, Song J, et al. Toxic effects of magnetic nanoparticles on normal cells and organs. *Life Sci*. 2019;220:156–161. doi:10.1016/j.lfs.2019.01.056
23. Malvindi MA, De Matteis V, Galeone A, et al. Toxicity assessment of silica coated iron oxide nanoparticles and biocompatibility improvement by surface engineering. *PLoS One*. 2014;9(1):e85835. doi:10.1371/journal.pone.0085835
24. Niemirowicz K, Piktel E, Wilczewska AZ, et al. Core-shell magnetic nanoparticles display synergistic antibacterial effects against Pseudomonas aeruginosa and Staphylococcus aureus when combined with cathelicidin LL-37 or selected ceragenins. *Int J Nanomedicine*. 2016;11:5443–5455. doi:10.2147/IJN.S113706
25. Surel U, Niemirowicz K, Marzec M, Savage PB, Bucki R. Ceragenins – a new weapon to fight multidrug resistant bacterial infections. *Studia Medyczne*. 2014;30(3):207–213. doi:10.5114/ms.2014.45428
26. Ding B, Guan Q, Walsh JP, et al. Correlation of the antibacterial activities of cationic peptide antibiotics and cationic steroid antibiotics. *J Med Chem*. 2002;45(3):663–669. doi:10.1021/jm0105070
27. Markiewicz K, Zembko P, Półtorak K, et al. Magnetic nanoparticles with chelating shells prepared by RAFT/MADIX polymerization. *New J Chem*. 2016;40:9223–9231. doi:10.1039/C6NJ01938B
28. Wilczewska AZ, Markiewicz KH. Surface-Initiated RAFT/MADIX Polymerization on Xanthate-Coated Iron Oxide Nanoparticles. *Macromol Chem Phys*. 2014;215(2):190–197.
29. Chou TC. Theoretical basis, experimental design, and computerized simulation of synergism and antagonism in drug combination studies. *Pharmacol Rev*. 2006;58(3):621–681. doi:10.1124/pr.58.3.10
30. Niemirowicz K, Durnaś B, Tokajuk G, et al. Formulation and candidacidal activity of magnetic nanoparticles coated with cathelicidin LL-37 and ceragenin CSA-13. *Sci Rep*. 2017;7(1):4610. doi:10.1038/s41598-017-04653-1
31. Sosa Iglesias V, Giuranno L, Dubois LJ, Theys J, Vooijs M. Drug resistance in non-small cell lung cancer: a potential for NOTCH targeting? *Front Oncol*. 2018;8:267. doi:10.3389/fonc.2018.00267

32. Van der Jeught K, Xu HC, Li YJ, Lu XB, Ji G. Drug resistance and new therapies in colorectal cancer. *World J Gastroenterol*. 2018;24 (34):3834–3848. doi:10.3748/wjg.v24.i34.3834
33. Wnorowska U, Fiedoruk K, Piktel E, et al. Nanoantibiotics containing membrane-active human cathelicidin LL-37 or synthetic ceragenins attached to the surface of magnetic nanoparticles as novel and innovative therapeutic tools: current status and potential future applications. *J Nanobiotechnol*. 2020;18(1):3. doi:10.1186/s12951-019-0566-z
34. Campos SM, Penson RT, Mays AR, et al. The clinical utility of liposomal doxorubicin in recurrent ovarian cancer. *Gynecol Oncol*. 2001;81(2):206–212. doi:10.1006/gyno.2000.5980
35. Khan MA, Zafaryab M, Mehdi SH, Ahmad I, Rizvi MM. Characterization and anti-proliferative activity of curcumin loaded chitosan nanoparticles in cervical cancer. *Int J Biol Macromol*. 2016;93(Pt A):242–253. doi:10.1016/j.ijbiomac.2016.08.050
36. Kuruvilla SP, Tiruchinapally G, Crouch AC, ElSayed MEH, Greve JM. Dendrimer-doxorubicin conjugates exhibit improved anticancer activity and reduce doxorubicin-induced cardiotoxicity in a murine hepatocellular carcinoma model. *PLoS One*. 2017;12(8): e0181944. doi:10.1371/journal.pone.0181944
37. Prylutska S, Grynyuk I, Matyshevska O, et al. C60 fullerene as synergistic agent in tumor-inhibitory Doxorubicin treatment. *Drugs R D*. 2014;14(4):333–340. doi:10.1007/s40268-014-0074-4
38. Hekmat A, Saboury AA, Divsalar A. The effects of silver nanoparticles and doxorubicin combination on DNA structure and its antiproliferative effect against T47D and MCF7 cell lines. *J Biomed Nanotechnol*. 2012;8(6):968–982. doi:10.1166/jbn.2012.1451
39. Durnaś B, Piktel E, Wątek M, et al. Anaerobic bacteria growth in the presence of cathelicidin LL-37 and selected ceragenins delivered as magnetic nanoparticles cargo. *BMC Microbiol*. 2017;17(1):167. doi:10.1186/s12866-017-1075-6
40. Tao X, Gou J, Zhang Q, et al. Synergistic breast tumor cell killing achieved by intracellular co-delivery of doxorubicin and disulfiram via core-shell-corona nanoparticles. *Biomater Sci*. 2018;6 (7):1869–1881. doi:10.1039/C8BM00271A
41. Karuppaiah A, Siram K, Selvaraj D, Ramasamy M, Babu D, Sankar V. Synergistic and enhanced anticancer effect of a facile surface modified non-cytotoxic silver nanoparticle conjugated with gemcitabine in metastatic breast cancer cells. *Mater Today Commun*. 2019;23:100884.
42. Zhang R, Wang X, Wu C, et al. Synergistic enhancement effect of magnetic nanoparticles on anticancer drug accumulation in cancer cells. *Nanotechnology*. 2006;17(14):3622–3626. doi:10.1088/0957-4484/17/14/043
43. Yin PT, Pongkulapa T, Cho HY, et al. Overcoming chemoresistance in cancer via combined microRNA therapeutics with anticancer drugs using multifunctional magnetic core-shell nanoparticles. *ACS Appl Mater Interfaces*. 2018;10(32):26954–26963. doi:10.1021/acsami.8b09086
44. Alarifi S, Ali D, Alkahtani S, Alhader MS. Iron oxide nanoparticles induce oxidative stress, DNA damage, and caspase activation in the human breast cancer cell line. *Biol Trace Elem Res*. 2014;159(1–-3):416–424. doi:10.1007/s12011-014-9972-0
45. Wu W, Chen B, Cheng J, et al. Biocompatibility of Fe3O4/DNR magnetic nanoparticles in the treatment of hematologic malignancies. *Int J Nanomedicine*. 2010;5:1079–1084. doi:10.2147/IJN.S15660
46. Ruden S, Hilpert K, Berditsch M, Wadhwani P, Ulrich AS. Synergistic interaction between silver nanoparticles and membrane-permeabilizing antimicrobial peptides. *Antimicrob Agents Chemother*. 2009;53 (8):3538–3540. doi:10.1128/AAC.01106-08